Supplementary Material for Article:

"The Excited-State Structure, Vibrations, Lifetimes and Nonradiative Dynamics of Jet-Cooled 1-Methylcytosine"

by Maria A. Trachsel, Timo Wiedmer, Susan Blaser, H.M. Frey, Quansong Li, Sergi Ruiz-Barragan, Lluís Blancafort and Samuel Leutwyler

A. Synthesis of 1-Methylcytosine

0.258 g KOH (4.6 mmol, 1.02 eqv.) were dissolved in 30 ml ethanol (absolute, 99.8%) and added to 0.496 g cytosine (4.5 mmol, 1 eq, Sigma Aldrich, $>$ 99%) under vigorous stirring. While cooling the mixture with ice, 0.29 ml iodomethane (0.65 g, 4.6 mmol, 1.02 eq.) were added. After reflux for 45 min, the solution was let to stand over night under continuous stirring. The white precipitate was dried under vacuum, yielding 186 mg (32%) of white powder. ^{1}H-NMR (300 MHz, DMSO-d_6): δ 7.56 (d, J = 7.14 Hz, 1 H, Ar); 6.94 (broad, 2 H, NH_2); 5.61 (d, J = 7.11 Hz, 1 H, Ar); 3.19 (s, 3 H, CH_3). These values are in agreement with previously published data.[1]

B. Synthesis of 1-(d_3)Methylcytosine

0.276 g KOH (4.9 mmol, 1.09 eqv.) were dissolved in 30 ml ethanol abs. (99.8%) and added to 0.500 g cytosine (4.5 mmol, 1 eqv., Sigma-Aldrich, $>$ 99%) under vigorous stirring. While cooling the mixture with ice, 0.31 ml iodomethane-d_3 (0.72 g, 5.0 mmol, 1.11 eq., Sigma-Aldrich, stab. with copper) were added. After reflux for 45 min, the solution was allowed to stand over night under continuous stirring. After cooling in the fridge for 8 hours, the white precipitate was dried under vacuum, yielding 328 mg (52%) of white powder. ^{1}H-NMR (300 MHz, DMSO-d_6): δ 7.56 (d, J = 7.11 Hz, 1 H, Ar); 6.93 (broad, 2 H, NH_2); 5.61 (d, J = 7.14 Hz, 1 H, Ar).

C. Additional Computational Details

C1. Active space selection. To apply the MS-CASPT2//CASSCF approach successfully, strong differential correlation effects at the CASSCF level must be avoided. This occurs when there are large differences in the correlation energy provided by MS-CASPT2 with respect to CASSCF for the different states. It can result in changes in the order of the states from CASSCF to MS-CASPT2, discontinuities in the MS-CASPT2//CASSCF energy profiles and large MS-CASPT2 energy gaps at the CASSCF optimized intersections. To avoid these issues, the active space for the CASSCF calculations has been chosen with the aim of minimizing the MS-CASPT2 S_1/S_0 energy gap at the conical intersections. To achieve this goal, orbitals

with 3p character were included to account for radial correlation of orbitals which have occupation close to two in one state and are singly occupied in the other state, similar to what is described in Ref. 2. Following these ideas, for the path to $(Eth)_X$ we use a (10,10) active space including 7 π orbitals (4 occupied and 3 empty ones), the σ and $\sigma*$ orbitals of the twisted C_5-C_6 bond and a 3p orbital on C_5. For the path to $(OP)_X$, the active space is (12,12) and includes 7 π orbitals, two pairs of σ,$\sigma*$ orbitals localized on the C_2-N_3 and N_3-C_4 bonds, respectively, and a 3p orbital on N_3. The MS-CASPT2 energies along the paths were obtained with the active spaces used to optimize each path, state-averaging over two and three states for the path to $(Eth)_X$ and $(OP)_X$, respectively. To obtain the barriers along the two paths, structure $^1(\pi,\pi^*)_{Min}$ was reoptimized in each case with the active space used for the calculation of the path and the MS-CASPT2 energy recalculated accordingly. The barriers also include the zero-point energy (ZPE) correction based on frequency calculations at $^1(\pi,\pi^*)_{Min}$ and the corresponding TS.

C2. Reaction path calculations. The TS between the S_1 minimum, $^1(\pi,\pi*)_{Min}$, and $(Eth)_X$ was optimized and characterized with a numerical frequency calculation, and the reaction path was optimized with the intrinsic reaction coordinate (IRC) method.[3] In its turn, the first part of the path to $(OP)_X$ goes from $^1(\pi,\pi*)_{Min}$ to a minimum on S_1, $(OP)_{Min}$. The TS between the two minima was optimized and characterized with a numerical frequency calculation, and the reaction path from the TS to $^1(\pi,\pi*)_{Min}$ was optimized with the IRC method. In contrast to this, the IRC calculation to $^1(OP)_{Min}$ was unsuccessful and the reaction path was approximated with a linear interpolation in internal coordinates. The minimum energy path from $(OP)_X$ to $^1(OP)_{Min}$ was also calculated with the IRC method. In this case, the initial direction of the IRC was determined with the initial relaxation direction (IRD) algorithm.[4]

TABLE I. Table SI1. MS-CASPT2 S_0 and S_1 absolute energies in hartree of the $^1(\pi,\pi*)_{Min}$ obtained with different methods. Ring puckering described by $|\delta|$.[a]

Method	E_0	E_1	$\lvert\delta\rvert$
TD-CAM-B3LYP/6-311G**	-433.28474	-433.15511	15.8
CASSCF(12,11)/6-311G**	-433.28353	-433.15361	7.0
MS-CASPT2(8,7)/DZP [b]	-433.28262	-433.15157	14.5
TD-B3LYP/6-311G**	-433.27273	-433.15030	2.6
SCS-CC2/aug-cc-pVDZ	-433.26714	-433.14954	14.3
CASSCF(10,8)/6-311G**	-433.2756	-433.14966	2.4
CC2/aug-cc-pVDZ	-433.26674	-433.14612	1.6

[a] Average of the unsigned six ring dihedral angles. A value $|\delta| = 0$ corresponds to a perfectly planar ring.
[b] Ref. 5.

D. UV/UV Depletion Spectra

In UV/UV holeburning and depletion spectroscopy negative-going bands are usually observed, because the holeburning or depletion laser depopulates the S_0 state $v'' = 0$ level, thereby *reducing* the signal of the 2C-R2PI detection laser at later time (300 ns delay, see Section II). Quite unusually, the UV/UV depletion spectra of 1MCyt and 1-(d_3)-MCyt show both *positive-* and negative-going bands. Figure 1(c) displays the UV/UV depletion spectrum of 1MCyt in comparison to the two-color R2PI spectrum in Figure 1(a) and the UV holeburning spectrum in Figure 1(b). The unusual positive-going bands in the UV/UV depletion

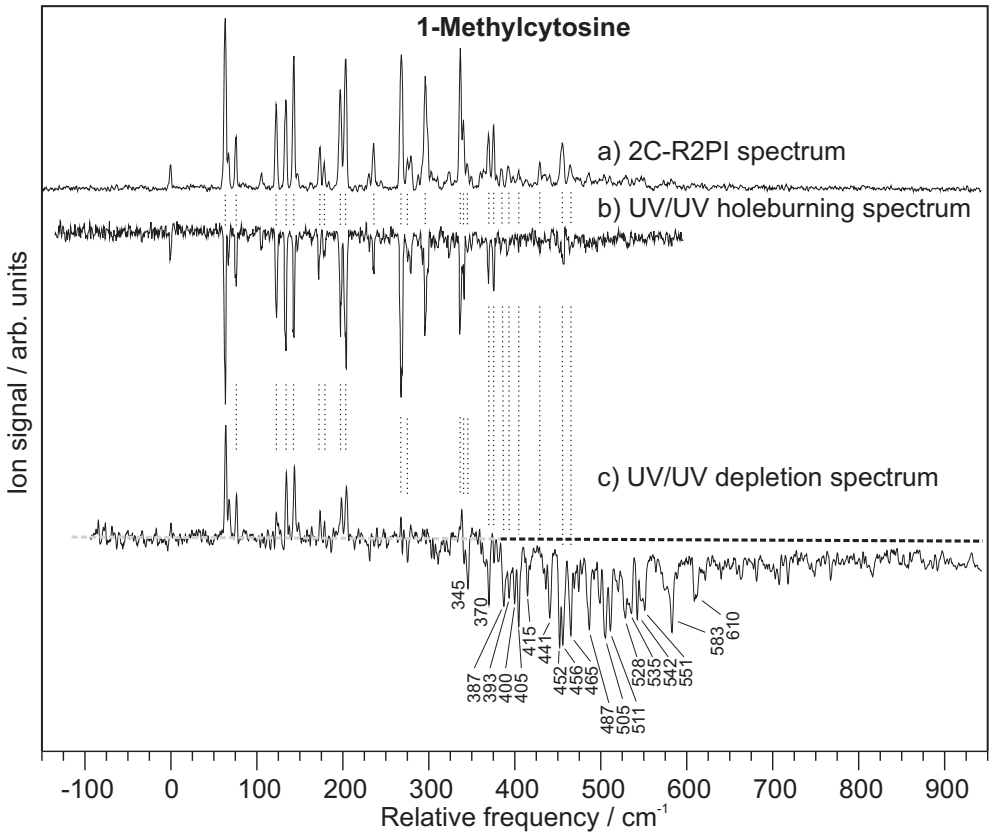

FIG. 1. FIG S1: (a) Two-color resonant two-photon ionization spectrum, (b) UV/UV holeburning spectrum and (c) UV/UV depletion spectrum of keto-amino 1-methylcytosine; the scale is relative to the 0_0^0 band at 31852 cm^{-1}. In the UV/UV holeburning spectrum (b) the depletion laser was set to the band at 0_0^0+455 cm^{-1}. In the UV/UV depletion spectrum (c) the detection laser was set to the intense vibronic band at 0_0^0+64 cm^{-1}.

spectrum between 0 and $+210$ cm^{-1} arise from the relatively high efficiency of ISC relative to that of IC in 1MCyt. The molecules that cross to T_1 are long-lived and remain excited even after the depletion↔detection delay of 300 ns. Thus, as the depletion laser sweeps across a given UV band of 1MCyt, the 2C-R2PI detection signal decreases on one hand due to the depleted $S_0; v'' = 0$ population, but increases on the other hand due to the contribution from the long-lived T_1 molecules. The net signal in the UV depletion spectrum can then be positive or negative, depending on factors such as the delay time between depletion and detection, the lifetime of the T_1 levels, the relative ionization cross sections of the S_1 and T_1 molecules and the relative

rate of the ISC and IC nonradiative processes. Since we have determined the k_{ISC} and k_{IC} values as a function of vibrational energy in the S_1 state, see Table IV in the main paper, we here discuss the last factor. We show that (1) the UV depletion spectrum is consistent the values in Table IV, and (2) the UV depletion spectrum effectively constrains the relative ratio of the k_{ISC} and k_{IC} rates.

From Table IV we see that k_{ISC}:k_{IC} is $\sim 30\%$ at the $+66$ cm^{-1} vibrational level, decreasing to $\sim 5\%$ at $+201$ cm^{-1} and further to $\sim 2\%$ at the $+274$ cm^{-1} level. The corresponding bands in the UV depletion spectrum, Figure 1(c), have strong, medium and small intensity (note that the errors of these ratios are rather large, given the 1σ errors of k_{ISC} and k_{IC} in Table IV). Although we could not measure reliable k_{ISC} or k_{IC} values for the S_1 state $v' = 0$ level, due to the small Franck-Condon factor of the 0_0^0 band, we estimate that k_{ISC}:$k_{IC} > 30\%$ at the $v' = 0$ level, since the 0_0^0 band is clearly positive-going in Figure 1(c). The bands in the UV depletion spectrum go to zero at about 340 cm^{-1}, right in the middle of a group of intense bands, see the 2C-R2PI spectrum Figure 1(a). The lowest of these bands at $+335$ cm^{-1} is positive, while the $+345$ cm^{-1} band goes negative. At this energy Table IV shows that k_{ISC}:$k_{IC} \sim 3\%$. At vibrational energies above $+345$ cm^{-1}, all the bands in the UV depletion spectrum are negative-going.

For these higher-energy bands, the k_{ISC}:k_{IC} values from Table IV are in a range of $1.7 - 5.6\%$. As noted above, the 1σ errors are Table IV are large. If we apply the 1σ errors, the 5.6% value for the level at $+401$ cm^{-1} varies from between 1.9% and 12%. Clearly, k_{ISC}:k_{IC} values above 3% are not compatible with a negative-going bands, as discussed above. Thus, the UV depletion spectrum could be used to limit the k_{ISC}:k_{IC} ratios in Table IV to values that are consistent with the spectrum. We will not do this in detail, but we point out that above $+340$ cm^{-1} vibrational energy, only k_{ISC}:k_{IC} values $< 3\%$ are compatible with the UV depletion spectrum. Given the nearly monotonic decrease of k_{ISC}:k_{IC} with increasing energy in the range $0 - 340$ cm^{-1}, we expect that the true k_{ISC}:k_{IC} value approaches 1.5% at 516 cm^{-1}, which is the last value in Table IV.

The UV/UV depletion spectrum of 1-d_3-MCyt shown in Figure S3(c), was measured in the same way as the spectrum for 1MCyt, but here the detection laser was fixed at the intense band at +292 cm^{-1}. The appearance of positive-going bands in the depletion spectrum and the switching to negative-going bands above $+307$ cm^{-1} is consistent with that for undeuterated 1MCyt. We have not measured the k_{ISC} and k_{IC} values for 1-d_3-MCyt, and the UV depletion spectrum does not give further information on their ratio.

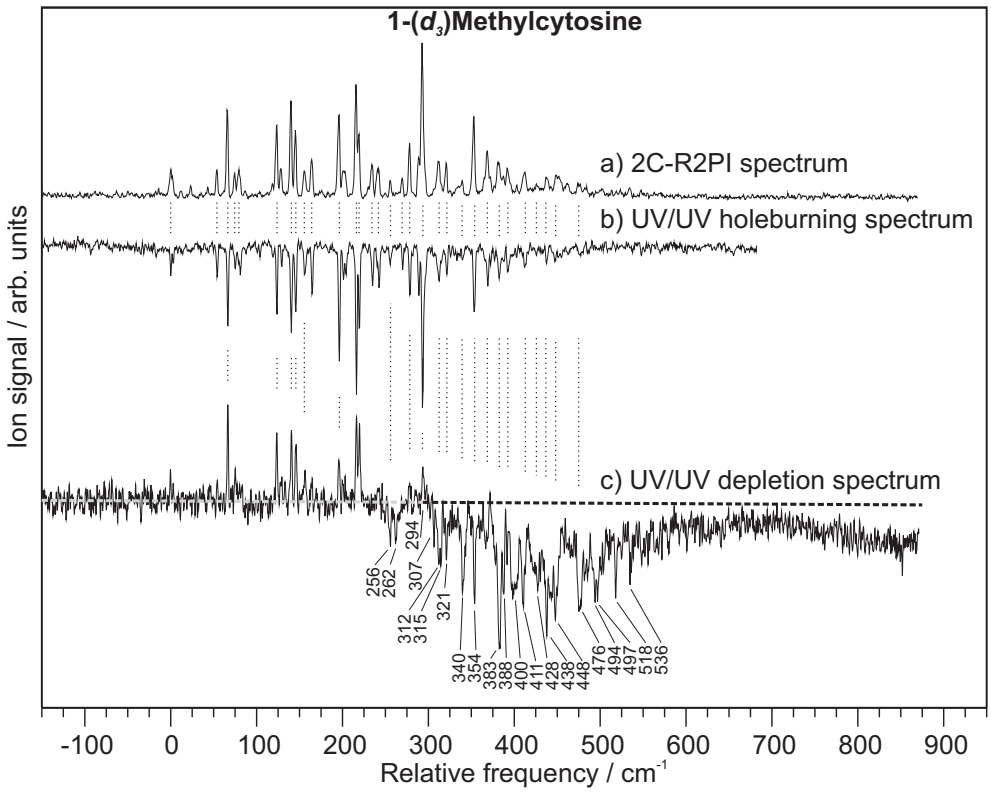

FIG. 2. FIG S3: (a) Two-color resonant two-photon ionization spectrum, (b) UV/UV holeburning spectrum and (c) UV/UV depletion spectrum of keto-amino 1-d_3-methylcytosine; the scale is relative to the 0_0^0 band at 31925 cm^{-1}. In the UV/UV holeburning spectrum (b) the depletion laser was set to the band at 0_0^0+381 cm^{-1}. In the UV/UV depletion spectrum (c) the detection laser was set to the intense vibronic band at 0_0^0+292 cm^{-1}.

E. Additional Spectra

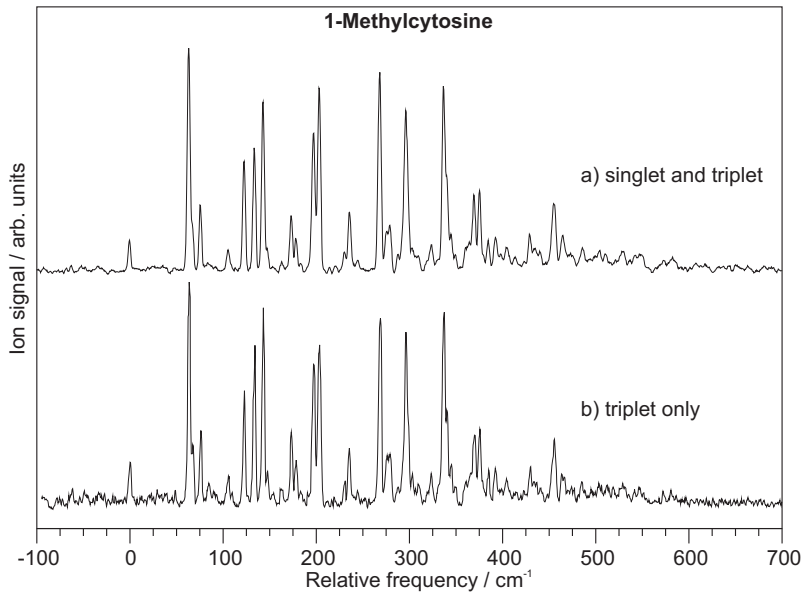

FIG. 3. FIG S4: (a) 2C-R2PI spectrum of 1-methylcytosine with prompt ionization at 223 nm; (b) with 30 ns delayed ionization at 215 nm, corresponding to ionization out of the triplet state.

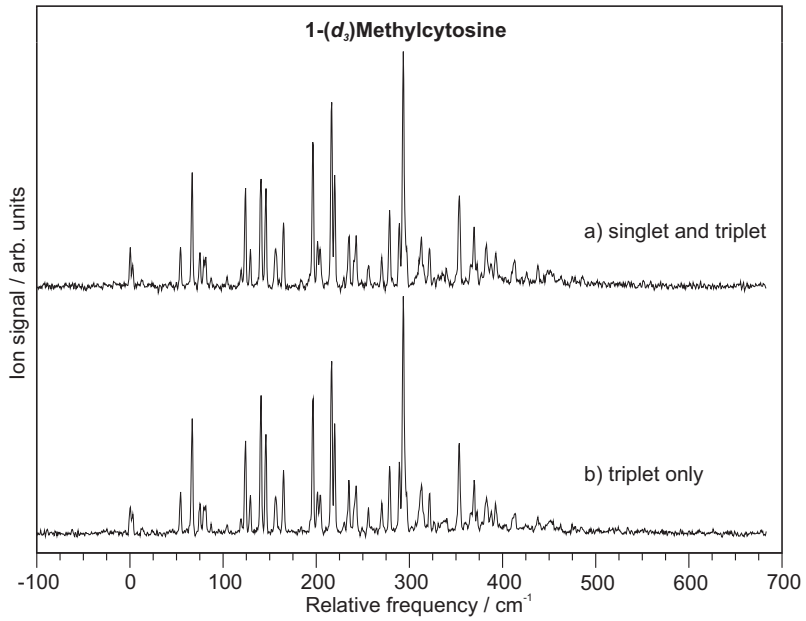

FIG. 4. FIG S5: (a) 2C-R2PI spectrum of 1-d_3-methylcytosine with prompt ionization at 223 nm; (b) with 30 ns delayed ionization at 215 nm, corresponding to ionization out of the triplet state.

F. Methyl Group Internal Rotation Potential

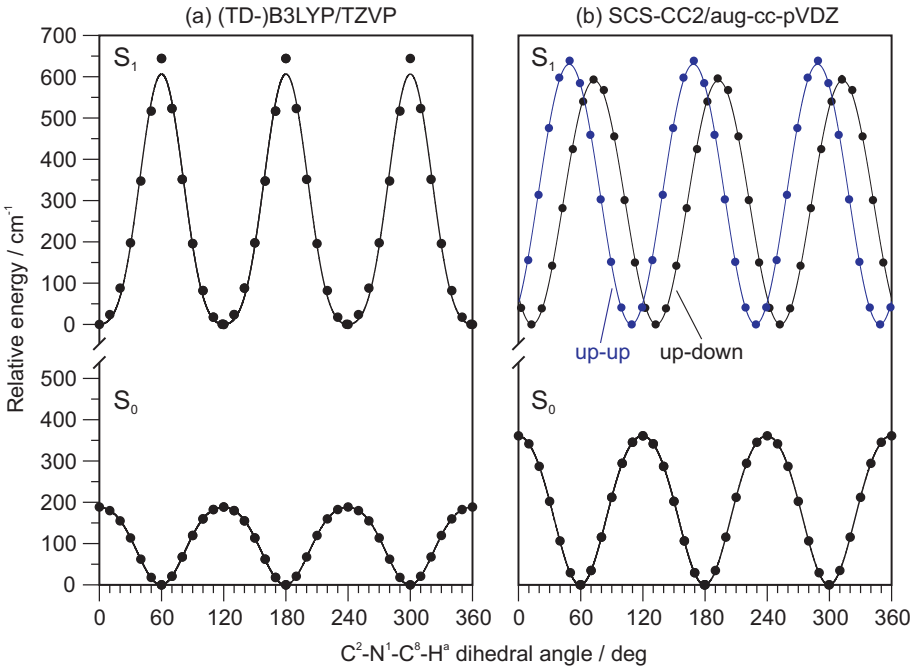

FIG. 5. FIG S6: (a) (TD-)B3LYP/TZVP and (b) SCS-CC2/aug-cc-pVDZ calculated (dots) and fitted (lines) S_0 and S_1 state methyl internal rotation potentials for 1MCyt. In the SCS-CC2 S_1 state two ring-puckering conformers with slightly different barrier heights exist, see text. To obtain a S_1 potential of a pure methyl torsional motion, the N^3-C^2-N^1-C^6 and C^6-C^5-C^4-N^3 dihedrals (butterfly angle) had to be fixed, all other parameters were optimized.

[1] Papoulis, A.; Al-Abed, Y.; Bucala, R. *Biochemistry* **1995**, *34*, 648–655.

[2] Blancafort, L. *J. Photochem. Photobiol.* **2007**, *83*, 603–610.

[3] González, C.; Schlegel, H. B. *J. Phys. Chem.* **1990**, *94*, 5523–5527.

[4] Celani, P.; Robb, M. A.; Garavelli, M.; Bernardi, F.; Olivucci, M. *Chem. Phys. Lett.* **1995**, *243*, 1–8.

[5] Nakayama, A.; Yamazaki, S.; Taketsugu, T. *J. Phys. Chem. A* **2014**, *118*, 9429–9437.